

Geophysical Research Letters[®]

RESEARCH LETTER

10.1029/2021GL097579

Special Section:

Southern Ocean clouds, aerosols, precipitation and radiation

Key Points:

- Sea surface temperature (SST) in Southern Ocean has a significant cooling trend in 1982–2020, with the largest trend in the central-east Pacific sector
- Surface shortwave radiation and Ekman horizontal advection are the two key factors to the SST cooling in the central-east Pacific sector
- Reduced downward shortwave radiation is attributed to the increase of total cloud cover, which enhances shortwave cloud-radiative feedback

Supporting Information:

Supporting Information may be found in the online version of this article.

Correspondence to:

J. Liu,
jliu26@albany.edu




Citation:

Xu, X., Liu, J., & Huang, G. (2022). Understanding sea surface temperature cooling in the central-east Pacific sector of the Southern Ocean during 1982–2020. *Geophysical Research Letters*, 49, e2021GL097579. <https://doi.org/10.1029/2021GL097579>

Received 4 JAN 2022

Accepted 11 MAY 2022

Understanding Sea Surface Temperature Cooling in the Central-East Pacific Sector of the Southern Ocean During 1982–2020

Xiaoqi Xu^{1,2} , Jiping Liu³ , and Gang Huang^{1,2} 

¹State Key Laboratory of Numerical Modeling for Atmospheric Sciences and Geophysical Fluid Dynamics, Institute of Atmospheric Physics, Chinese Academy of Sciences, Beijing, China, ²University of Chinese Academy of Sciences, Beijing, China, ³Department of Atmospheric and Environmental Sciences University at Albany, State University of New York, New York, NY, USA

Abstract Sea surface temperature (SST) in the Southern Ocean plays an important role in air-sea interactions, forcing atmospheric variability. Using various observational and reanalysis data sets, we show that the SST cooling trend in the Southern Ocean (50°S–70°S) continues (~0.3°C from 1982 to 2020). The largest SST cooling trend is in the central-east Pacific sector, which can extend to 250 m. A detailed trend analysis for the mixed layer heat budget equation suggests that changes in the net surface shortwave radiation and Ekman horizontal advection are the two key contributors, though the other processes contribute to the SST cooling trend in winter and spring. The reduced downward solar radiation is largely due to the increase of cloud cover, which enhances shortwave-cloud-radiative feedback and decreases SST. Changes in Ekman advection associated with increased zonal winds is in favor of the colder water remaining in upper ocean layer.

Plain Language Summary Despite the critical role of the Southern Ocean in global climate, it has remained poorly observed compared to other oceans. SST in the Southern Ocean is considered as an important indicator of climate change. This study shows that the Southern Ocean (50°S–70°S) sea surface temperature has a significant and robust cooling trend during 1982–2020, with the largest cooling trend in the central-east Pacific sector, which is supported by different SST data sets. Our further analysis reveals that the SST cooling is primarily the result of two processes. One is the decrease of surface downward shortwave radiation caused by the increased total cloud cover that reflects more shortwave radiation to the space. The other is changes in Ekman transport associated with the intensified zonal winds that transport more cold water northward and suppress the upwelling of the subsurface warmer water. The other processes might contribute to the SST cooling trend in specific seasons.

1. Introduction

The Southern Ocean is a highly complex and critically important component of the global climate system for its ability to take up heat and carbon dioxide, and thereby mitigates human-induced global warming. Sea surface temperature (SST) plays a key role in ocean-atmosphere interactions, forcing atmospheric variability. In contrast to the global warming, it has been reported that SST in the Southern Ocean has decreased since the satellite observations began (Armour et al., 2016; Jones et al., 2016; Rye et al., 2020), that is, the SST decreasing trend is ~0.05°C per decade averaged between 50°S and 70°S during 1979–2012 (Zhang et al., 2019) and ~0.06°C per decade averaged between 55°S and 70°S during 1982–2014 (Kostov et al., 2017).

Understanding of the mechanisms underlying the SST decreasing trend in the Southern Ocean is important for improving Southern Ocean simulation in climate models and predicting future Southern Ocean climate change. Some studies have suggested that the decreased SST is induced by a poleward intensification of the westerlies (Bitz & Polvani, 2012; Hall & Visbeck, 2002; Sen Gupta et al., 2009). Hall and Visbeck (2002) showed that the positive Southern Annual Mode (SAM) induced anomalous northward Ekman transport, it may result in the SST cooling south of 50°S. By contrast, using the Community Climate System Model version 3.5 model, Bitz and Polvani (2012) concluded that the ozone-driven poleward intensification of the westerlies leads to an increase of SST in the Southern Ocean. Using two different climate models, Ferreira et al. (2015) showed that the SST response to winds related to the ozone depletion has two-time-scale behaviors. The fast response is mediated by the mixed layer dynamics and air-sea interaction, driven by Ekman advection of colder water northward

associated with a positive SAM, while air-sea heat interactions act as a damping. The slow response is due to the interior ocean dynamics, sustained by Ekman upwelling of warmer water south of the Antarctic Circumpolar Current. Kostov et al. (2017) used CMIP5 models to show that anomalous Ekman transport might affect the response to SAM on interannual and decadal timescales, and the SST response is nonmonotonic in time.

Some other studies suggested that the increasing of surface freshwater fluxes might be the potential cause of the surface cooling in the Southern Ocean, since the freshwater increases vertical density stratification and suppresses the upwelling of warmer subsurface waters (Haumann et al., 2020, 2016; Pauling et al., 2016; Purich et al., 2018). Using a global coupled climate model with additional freshwater applied to the Southern Ocean, Purich et al. (2018) showed that surface freshening could cause the cooling due to a reduction in ocean convection and weaken entrainment of warm subsurface waters into the surface layer. Haumann et al. (2020) concluded that most of the surface cooling and subsurface warming in the high-latitude Southern Ocean during 1982–2011 was primarily caused by the increased wind-driven sea-ice transport rather than the changes in the glacial melt water input or wind-driven ocean circulation and mixing changes.

Sen Gupta and England (2006) investigated the SST change in the Southern Ocean in response to the SAM using the heat budget and regression analysis, showing that air-sea heat flux and meridional advection are the two dominant processes. Sallée et al. (2010) and Vivier et al. (2010) also suggested that the temperature anomaly produced by the heat budget analysis is comparable to the observed SST anomaly associated with the SAM. However, the mechanisms leading to the long-term cooling trend in the Southern Ocean between early 1980s and early-2010s identified in the previous studies remain not well understood (Haumann et al., 2020).

The goal of this article attempts to answer the following two questions.

1. Does the observed SST cooling trend in the Southern Ocean continue to present in updated/improved observation and reanalysis data?
2. Which physical processes contribute to the largest SST cooling trend in the central-east Pacific sector of the Southern Ocean based on a detailed analysis of the mixed layer heat budget equation?

2. Data and Methods

2.1. Data

We use the monthly mean SST data from the National Oceanic and Atmospheric Administration Optimum Interpolation data set Version 2 with a spatial resolution of $1^\circ \times 1^\circ$ (OISST v2; Reynolds et al., 2002), which is a blended objective analysis of both in situ measurements and satellite observations. Two additional SST data are also used to confirm the analysis. One is the Hadley Center Sea Ice and SST data set with a spatial resolution of $1^\circ \times 1^\circ$ (HadISST1; Rayner et al., 2003), which combines the Met Office Marine Data Bank and International Comprehensive Ocean-Atmosphere Data Set (ICOADS), and also includes the SST data received through the Global Telecommunications System marine observations. The other is the NOAA Extended Reconstructed SST Version 5 with a spatial resolution of $2^\circ \times 2^\circ$ (ERSST v5; Boyin Huang et al., 2017), which is derived from ICOADS data. HadISST1 and ERSST v5 can be considered as relatively independent data sets since both uses the ICOADS data. The European Center for Medium-Range Weather Forecasts (ECMWF) Ocean Reanalysis System 5 (ORAS5; Zuo, et al., 2019) is also used in this study, which is a new global eddy-permitting ocean-sea ice ensemble reanalysis system. The variables used here include ocean potential temperature, mixed layer depth, sea level height, and current velocity.

For the atmospheric data, 10 m wind speed is obtained from the fifth-generation ECMWF Reanalysis (ERA5; Hersbach et al., 2019), which combines extensive amounts of observations with advanced model and data assimilation system. To reduce the parameter uncertainty in the ERA5 data, we use the radiation, turbulent heat flux and cloud cover from the ensemble mean of ECMWF data, which consist of 10 ensemble members (Hersbach et al., 2019). A newly developed high-resolution version of the International Satellite Cloud Climatology Project (ISCCP-HGM; Young et al., 2017) is also used to facilitate the analysis, which is derived from a series of operational weather satellites, providing global record of cloud properties for the period of 1983–2016. Here, we use the radiation data to calculate the net shortwave radiation (SWnet) and the net longwave radiation (LWnet) at sea

surface, and define the cloud radiative effect (CRE) as the difference of between total-sky and clear-sky conditions (Alkama et al., 2020; Charlock & Ramanathan, 1985).

2.2. Methods

SST variability is driven by a number of processes which are often described by the terms of the ocean mixed layer heat budget equation (Dong et al., 2007; Qiu & Kelly, 1993; Sallée et al., 2010), including net shortwave and longwave radiation (the first two terms on the right side of Equation 1), sensible and latent heat fluxes (3rd and 4th terms), Ekman and geostrophic horizontal advection (5th and 6th terms), and diffusion in the mixed layer (7th term), and entrainment (the last term) at the base of the mixed layer.

$$\underbrace{\frac{\partial T}{\partial t}}_{\text{tendency}} = \underbrace{\frac{Q_{sw}}{\rho_0 C_p h_m} + \frac{Q_{lw}}{\rho_0 C_p h_m} + \frac{Q_{sh}}{\rho_0 C_p h_m} + \frac{Q_{lh}}{\rho_0 C_p h_m}}_{\text{net heat flux}} - \underbrace{\vec{V}_E \cdot \nabla T - \vec{V}_G \cdot \nabla T}_{\text{horizontal advection}} + \underbrace{\kappa_H \nabla^2 T}_{\text{diffusion}} + \underbrace{\frac{\partial h_m}{\partial t} \cdot (T_b - T)}_{\text{entrainment}} \quad (1)$$

Here T , T_b , and h_m denote SST, the temperature just below the mixed layer, and the depth of the mixed layer, respectively. Q_{sw} , Q_{lw} , Q_{sh} , and Q_{lh} are the net shortwave radiative flux, net longwave radiative flux, sensible heat flux, and latent heat flux, respectively. V_e and V_g are Ekman and geostrophic current velocities, respectively. ρ_0 is the reference density of seawater with the value of $1,027 \text{ kg m}^{-3}$, and C_p is the heat capacity of seawater with the value of $4,000 \text{ J} \cdot \text{kg}^{-1} \text{ K}^{-1}$. κ_H is the eddy diffusivity with the value of $500 \text{ m}^2 \text{ s}^{-1}$ in the Southern Ocean following (Dong et al., 2007). For simplification, the entrainment rate is calculated as the rate of change of the mixed layer depth. Here, we ignore the minor influence due to the absorption of downward shortwave radiation by the water through the mixed layer and vertical turbulent mixing. In this study, we analyze the trend of these terms to determine which are responsible for the identified SST trend.

3. Results

3.1. Linear SST Trend

Figures 1a–1c show the linear trend of SST in the Southern Ocean based on the observational data. The SST from OISST v2 shows a cooling trend in the latitudinal band of 50°S – 70°S , but more confined to the Antarctic coast in the eastern Indian Ocean and western Pacific Ocean sectors. The largest cooling trend is located in the central-east Pacific (50°S – 70°S , 180° – 60°W), where the maximum can reach about $-0.15^\circ\text{C/decade}$ (Figure 1a). This cooling trend is consistent to that reported in the previous study (Haumann et al., 2020), which shows the trend is about $-0.1^\circ\text{C/decade}$ during 1982–2011 between the ice edge and the subantarctic front in the Pacific sector. The SST trends from HadISST1 and ERSST5 exhibit similar pattern as that of the OISST v2, although the cooling trend of HadISST1 can extend further north in the Indian and western Pacific sectors (Figure 1b) while ERSST5 can extend to about 45°S in the central-east Pacific sector of the Southern Ocean. As for the amplitudes, the trend of HadISST1 is slightly smaller than those of OISST v2 and ERSST5 (Figure 1c), but is comparable to the trend during 1979–2014 in the central-east Pacific which reached about $-0.15^\circ\text{C/decade}$ (Kostov et al., 2017) and even about $-0.2^\circ\text{C/decade}$ during 1990–2014 based on HadISST (Rye et al., 2020). Consistently, the ORAS5 reanalysis shows a very similar SST trend map compared to that of OISST v2 (Figure 1a), although the amplitude of the cooling trend is much larger in the central-east Pacific (about $-0.30^\circ\text{C/decade}$; Figure 1d). Thus different SST data sets agree on the fact that a strong cooling trend appears in the central-east Pacific sector of Southern Ocean during 1982–2020.

Figure S1 in Supporting Information S1 shows the linear trend of potential temperature in the upper ocean averaged over the zonal belt of 55°S – 65°S . It appears that the decrease of temperature is not just at the sea surface. Along this zonal belt, the cooling trend can extend to about 250 m in the central-east Pacific sector (180° – 60°W) where the largest surface cooling trend is located, which is accompanied by warming trends below.

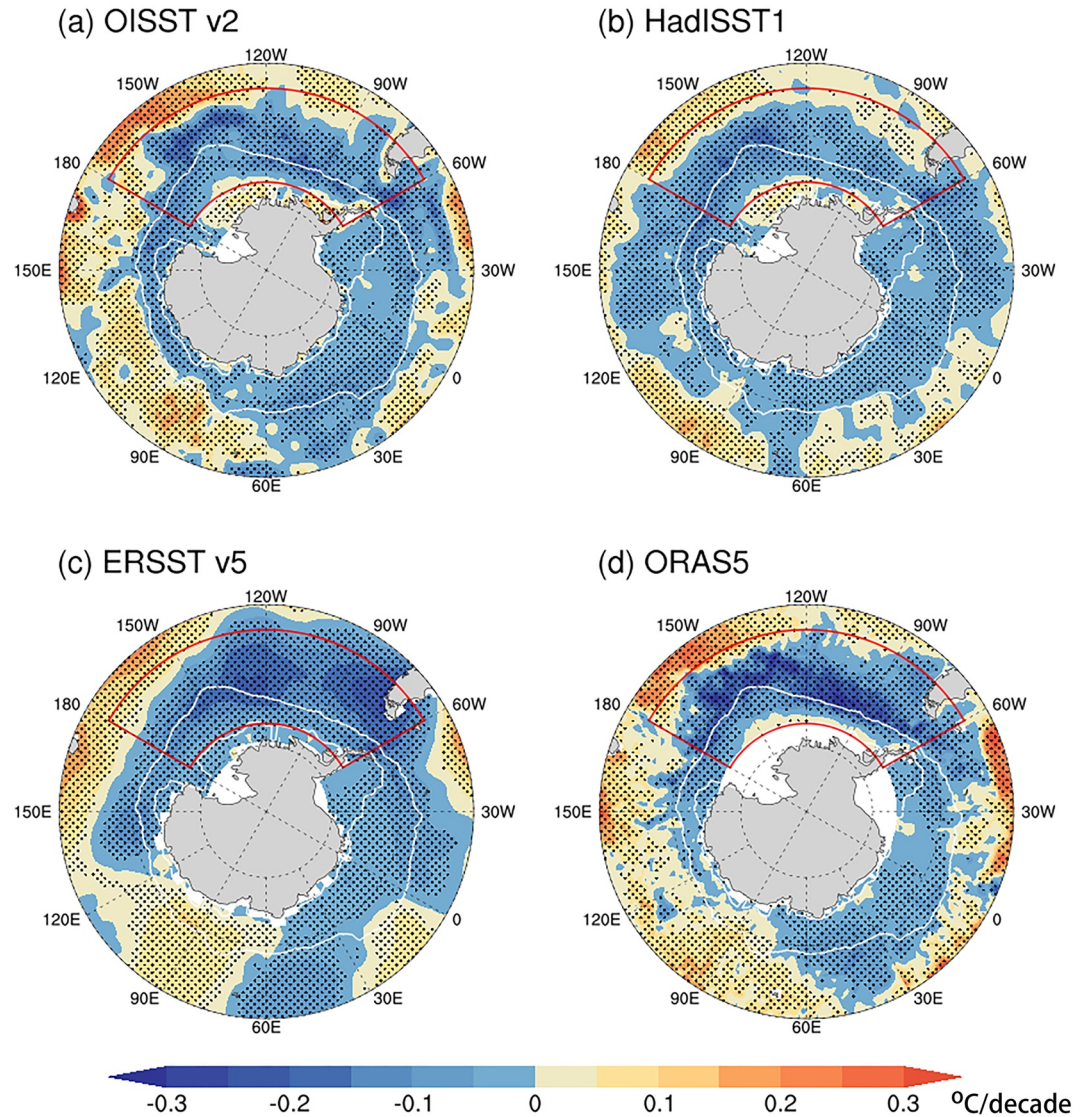


Figure 1. Sea surface temperature (SST) linear trend in the Southern Ocean: (a) OISST v2, (b) HadISST1, (c) ERSST v5, and (d) ORAS5 reanalysis during 1982–2020. (The dotting area is statistically significant at 95% confidence level using a Student's t test. The white lines outline the sea ice edge based on the contour of 15% sea ice concentration in September and February, separately.).

This is generally consistent with that the subsurface of the Southern Ocean became significantly warmer shown in previous studies (Armour et al., 2016; Haumann et al., 2020; Levitus et al., 2012).

3.2. Possible Causes of the SST Cooling in the Central-East Pacific Sector

Here, we focus on the central-east Pacific sector (50°S–70°S, 180°–60°W) to determine the possible processes which may cause the largest cooling trend there. First, we analyze the contribution of each individual surface heat flux to the observed SST trend, including shortwave radiation, longwave radiation, sensible heat flux, and latent heat flux. In this study, we used the following factors in descending order of importance to determine possible processes which may contribute to the largest cooling trend in the central-east Pacific sector, including (a) whether the spatial pattern of the SST trend associated with a specific process shows a broad cooling in the studying area, (b) whether the magnitude of the SST cooling associated with a specific process is closer to that of the observation shown in Figures 1 and 3) whether the SST cooling is statistically significant and has good areal coverage.

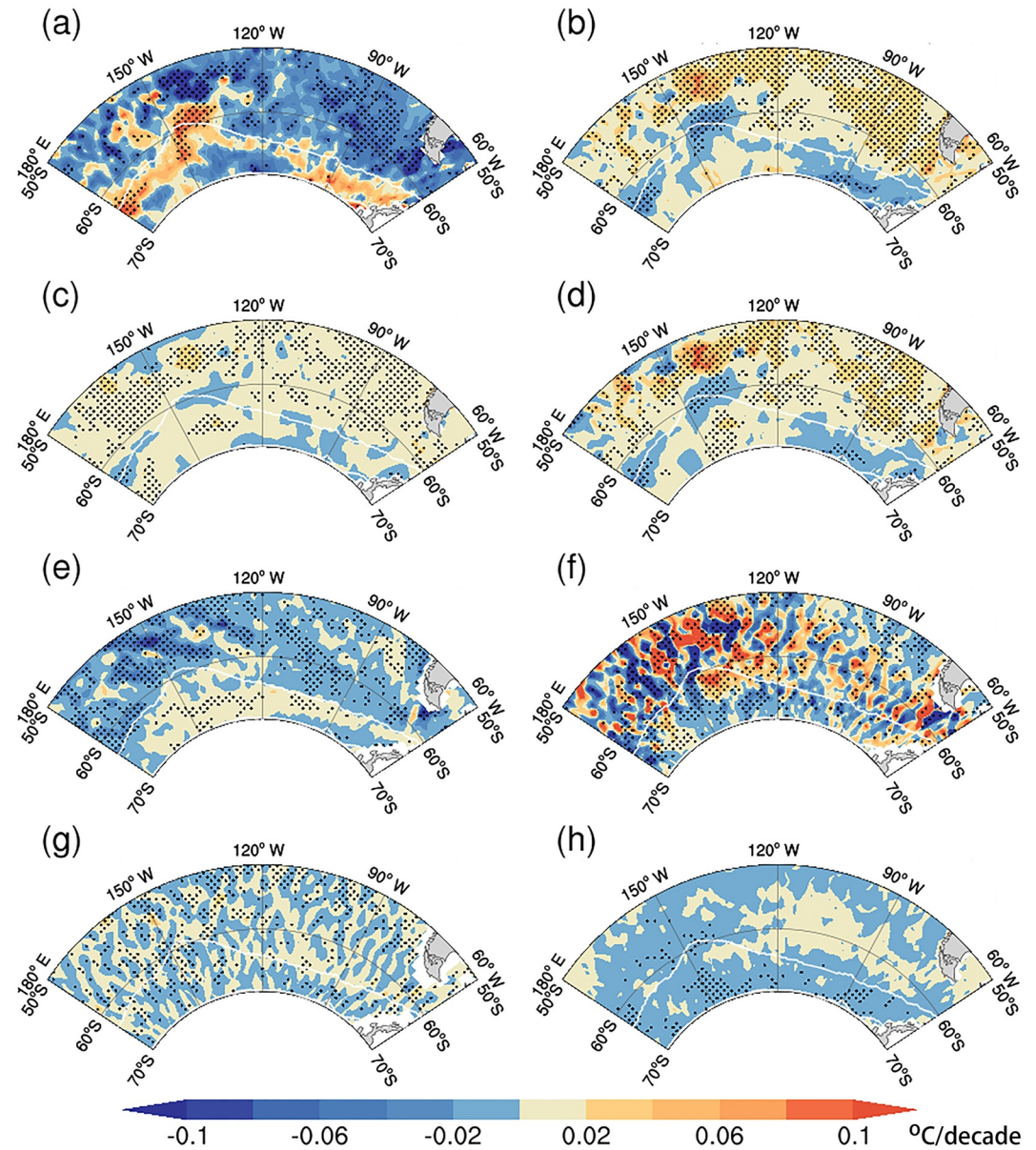


Figure 2. Sea surface temperature (SST) trend due to the change of surface heat flux: (a) net surface shortwave radiation, (b) net surface longwave radiation, (c) sensible heat flux, (d) latent heat flux, and oceanic dynamic processes: (e) horizontal Ekman advection, (f) horizontal geostrophic advection, (g) diffusion, and (h) entrainment during 1982–2020. (The dotting area is statistically significant at 95% confidence level using a Student's t test. The white lines outline the sea ice edge based on the contour of 15% sea ice concentration in September and February, separately.).

First, we analyze the contribution of each individual surface heat flux to the observed SST trend, including shortwave radiation, longwave radiation, sensible heat flux, and latent heat flux. As shown in Figures 2a–2d, among the four surface heat fluxes, the net shortwave radiation conforms to the spatial pattern of SST cooling trend with significantly decreasing trend in large parts of the central-east Pacific sector during 1982–2020, which is in favor of the SST cooling there. The cooling trend induced by the decreasing net shortwave radiation can reach about $-0.04^{\circ}\text{C}/\text{decade}$ in mostly central-east Pacific sector (Figure 2a). That means nearly one quarter of the SST cooling trend in the central-east Pacific sector might be explained by the change in the shortwave radiative flux. On the contrary, the SST change induced by the net longwave radiation, sensible and latent heat fluxes have opposite sign, which have a warming effect on SST (Figures 2b–2d). Next, we analyze the contribution of each individual ocean dynamic process to the observed SST trend, including horizontal Ekman advection, horizontal

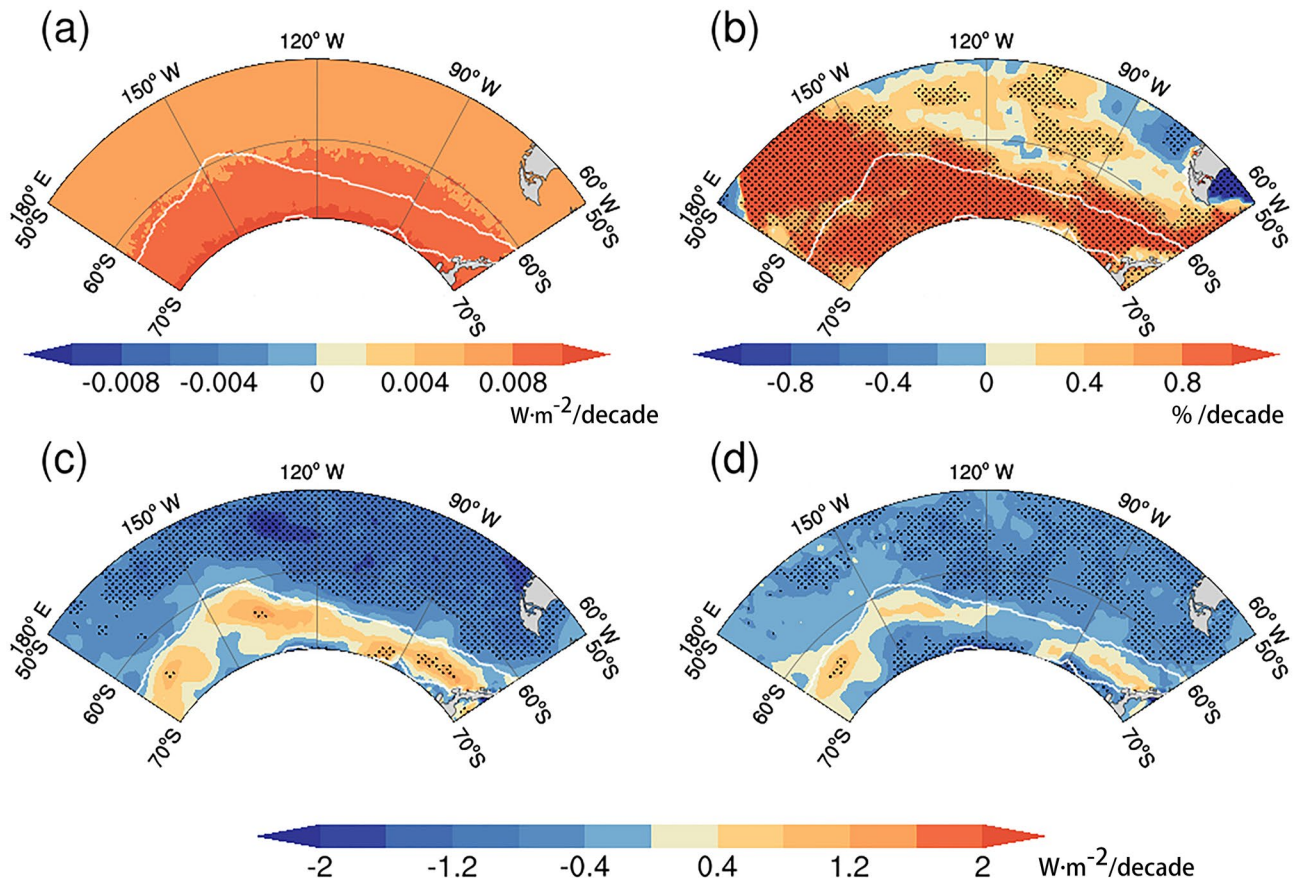


Figure 3. Trend of (a) incident solar radiation at the top of atmosphere from 10-ensemble mean of European Centre for Medium-Range Weather Forecasts (ECMWF) during 1982–2020, (b) total cloud cover (TCC) from ISCCP during 1984–2016, (c) shortwave cloud-radiative effect and (d) net cloud-radiative effect from 10-ensemble mean of ECMWF during 1982–2020. (The dotting area is statistically significant at 95% confidence level using a student's t test. The white lines outline the sea ice edge based on the contour of 15% sea ice concentration in September and February, separately.).

geostrophic advection, diffusion, and entrainment. As shown in Figures 2e–2h, the spatial distribution of the SST change induced by the Ekman current is broadly similar to that of the observed SST trend, with the largest cooling at around 150°W (Figure 2e), though its amplitude is relatively smaller than observed SST trend (mostly about $-0.02^{\circ}\text{C}/\text{decade}$) one-eighth of the SST cooling trend. By contrast, the distribution of the SST change induced by geostrophic advection is extremely non-uniform (alternating pattern) which does not conform to the observed SST trend pattern. This implies that it is not responsible for the observed SST trend (Figure 2f). The SST change associated with the diffusion is also non-uniform and the values are minimal (Figure 2g). Finally, the entrainment process produces minimal SST trend (Figure 2h), even though the SST change induced by entrainment has a cooling sign in parts of the central-east Pacific sector. The above analysis suggests that the change of the net shortwave radiative flux and Ekman horizontal advection are two primary processes contributing to the observed SST cooling trend in the central-east Pacific sector.

3.3. Underlying Mechanism for Changing Net Solar Radiation and Ekman Advection

As discussed above, the decrease of the net shortwave radiation at sea surface is an important factor for the SST cooling in the central-east Pacific sector. The question is what causes the decrease of surface net solar radiation. As shown in Figure 3a, the incident solar radiation at the top of the atmosphere has very minor change (near zero). This suggests that the solar radiation change occurs as it gets through the atmosphere (Kostov et al., 2017). As shown in Figure S2a in Supporting Information S1, the total cloud cover has increased over the central-east Pacific sector, which reflects solar radiation and cools sea surface, leading to the cooling in the central-east Pacific sector. We know an inherent problem of atmospheric reanalysis like ECMWF data is that cloud properties

are heavily modeled. Thus we also analyze the trend of the total cloud cover using the ISCCP satellite-derived data. It exhibits an increased trend over much of the central-east Pacific sector (Figure 3b). This conforms to the results from the 10 ensemble-mean of the ECMWF data. (Figures S2a and S2d in Supporting Information S1).

Figure 3c shows the trend of the shortwave cloud-radiative effect (SWcre). Negative values of SWcre are found over the central-east Pacific, which result in reduced shortwave radiation available to the sea surface. Such pattern is in good agreement with the cooling trend associated with the change of the net shortwave radiation. The increase of cloud cover may also warm sea surface through the longwave cloud-radiative effect (LWcre), which can partly offset the cooling effect of the shortwave cloud-radiative (SWcre). To assess the net effect of these two processes, the trend of the net cloud-radiative effect (NETcre) is shown in Figure 3d. Clearly, the central-east Pacific sector is still dominated by negative values of NETcre. This indicates that the net effect of increasing clouds ultimately cools the sea surface.

As discussed earlier, the SST cooling trend is also affected by meridional heat transport through Ekman advection driven by surface winds. There is a strengthening of zonal winds over most of the mid-to high-latitude ocean during 1982–2020. The largest strengthening occurs in the central-east Pacific sector and is located further north relative to the location of the largest SST cooling (Figure S4 in Supporting Information S1). The intensified zonal wind is consistent with variability of the Southern Annular Mode (SAM; Thompson et al., 2011). Fogt and Marshall (2020) showed that the annual mean SAM index has a significant positive trend in the past several decades. Moreover, the positive SAM trends are stronger in austral summer and autumn (Fogt & Marshall, 2020; Jones et al., 2009), which is consistent with the strongest SST cooling trend in summer associated with Ekman advection shown in Figure S5b in Supporting Information S1.

Climatologically, in the central-east Pacific sector, the westerly winds prevail north of 70°S and wind-driven Ekman advection transports colder water northwards. The maximum wind stress occurs at around 55°S that is in line with the strongest Ekman convergence in the upper ocean (Figure 4a). As shown in Figure S4 in Supporting Information S1, the positive trend of westerly winds in the central-east Pacific sector increases northwards in the past 40 yr. On the one hand, the Ekman advection enhances northward transport of cold water and extends the surface cooling further north. The maximum positive trend of the winds emerges north of 55°S (north of the maximum climatological westerly winds), which tends to reduce the meridional gradient of the winds north of 55°S and thus suppresses the Ekman convergence there. It is evident that the trend of vertical motion in the upper ocean has the opposite sign compared to that of the climatology, which favors the colder water remaining in the upper ocean layer (Figure 4b). On the other hand, the Ekman upwelling at 65°S is reduced, which limits the upward transport of warmer water from the deep ocean layer.

For SST, the trends in each season show the quite similar spatial pattern in the Southern Ocean with the largest cooling trend in the central-east Pacific sector (about $-0.3^{\circ}\text{C}/\text{decade}$), though the maximum cooling trend is more toward the eastern Pacific sector in the Southern Hemisphere summer (Figure S5b in Supporting Information S1). The contribution of downward shortwave radiation and Ekman advection to the SST cooling trend might be different among seasons, that is, the solar radiation has large seasonal cycle at mid-to-high latitudes, with large (minimal) solar radiation input in austral summer (winter). The other processes might play a role in some seasons. Figures S6–S9 in Supporting Information S1 show the spatial distribution and amplitude of the SST cooling trend associated with each individual parameter for four seasons. The strongest SST cooling associated with the net surface shortwave radiation is found in austral summer (Figure S7a in Supporting Information S1), with the maximum change located toward the east Pacific sector that is consistent with Figure S5b in Supporting Information S1. It has small effect on the SST in austral winter (Figure S9a in Supporting Information S1). Thus, the net shortwave radiation is a key contributor for the SST cooling in austral spring, summer, and autumn (Figures S6–S8 in Supporting Information S1). For horizontal Ekman advection, there is no distinct seasonal differences in the spatial distribution and amplitude of SST cooling trend (Figure S6e, S7e, S8e, and S9e in Supporting Information S1), but it exhibits a stronger contribution to the cooling trend in austral summer (Figure S7e in Supporting Information S1), which might be associated with the strongest positive seasonal SAM trend in austral summer (Fogt & Marshall, 2020). Additionally, we notice that in austral spring and summer, the entrainment tends to contribute to the SST cooling trend (Figures S6h and S7h in Supporting Information S1). In austral winter, the net longwave radiation and sensible and latent heat fluxes tend to contribute to some of the SST cooling trend, which compensates the reduced effect due to the minimal solar radiation input (Figure S9 in Supporting Information S1).

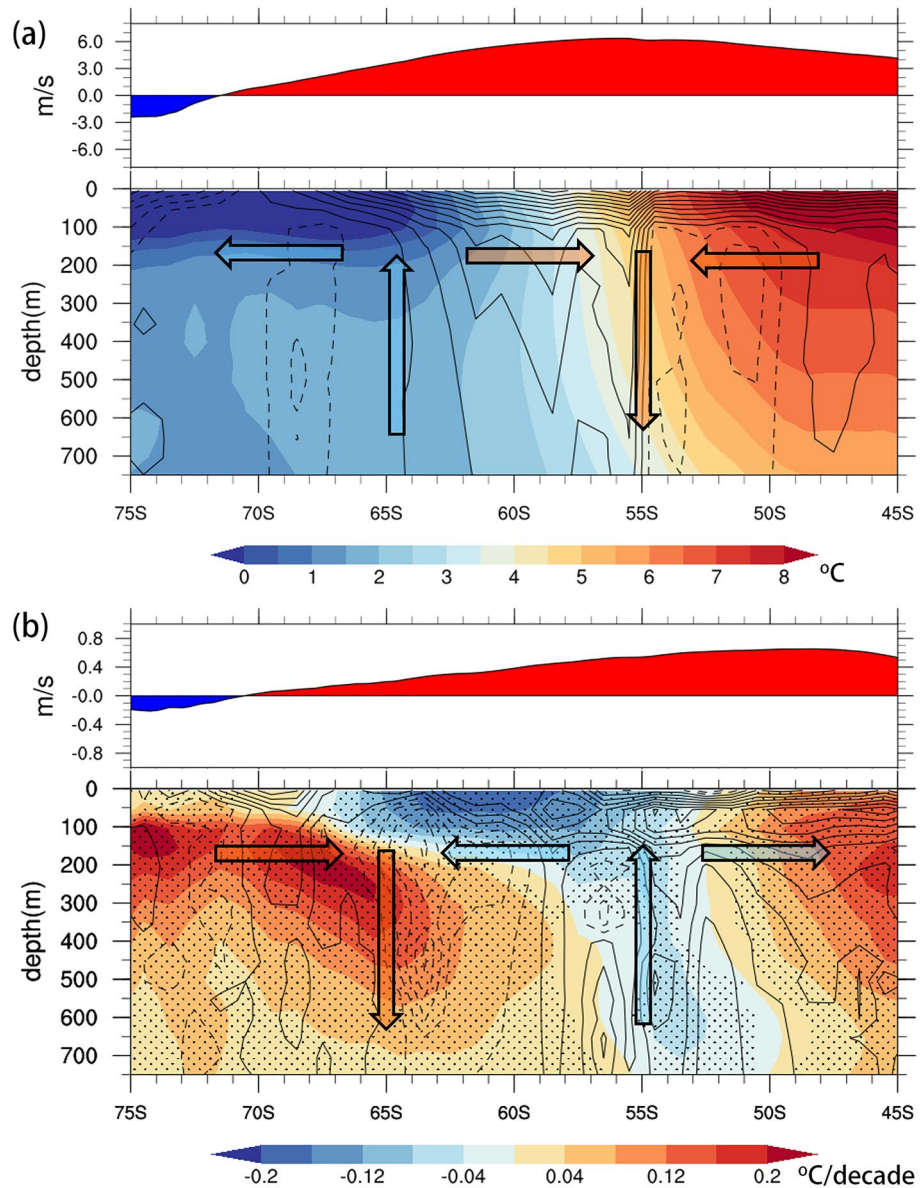


Figure 4. Change of zonal-mean (60°W–180°W) surface wind and ocean current: (a) Climatological zonal-mean 10 m zonal wind, and potential temperature from ORAS5, with contours of ocean meridional current in intervals of 0.002 m/s (The solid line represents northward, and the dashed line represents southward. The dotting area is statistically significant at 95% confidence level using a student's *t* test.). Arrows indicate the transport direction. (b) are the same as (a), but for trend over 1982–2020 and the contours are in intervals of 10^{-4} m/s/decade.

4. Discussion and Conclusion

In this study, the potential physical contributors responsible for the observed SST cooling in the central-east Pacific sector were investigated by analyzing the trend of each individual term in the mixed layer heat budget equation. Various observational and analysis data to exhibit that the cooling trend of SST in the Southern Ocean continues, and the averaged trend is about 0.3°C from 1982 to 2020. The largest SST cooling trend is located in the central-east Pacific sector of the Southern Ocean, which can extend to about 250 m. Our analyses in the central-east Pacific sector suggest that the net shortwave radiative flux and the wind-driven Ekman advection are two important factors contributing to the SST cooling there. The cooling effect associated with the net shortwave radiation flux is mainly attributed to the increase of the total cloud cover. It enhances the shortwave cloud-radiative feedback, which cools the SST by reflecting more shortwave radiation. As shown in Figure S2b in Supporting

Information S1, the 10 ensemble-mean of the ECMWF data suggests that the positive trend of total cloud cover is largely due to the increased low-level cloud cover over the central-east Pacific, whereas ISCCP suggests that the mid-level cloud cover is the most important contributor to the increased total cloud cover (Figures S3a and S3b in Supporting Information S1). Thus we cannot conclude whether the decrease of downward shortwave radiation is due to the increase of low-level or mid-level cloud cover. As for the changes in Ekman transport, they are associated with the intensified zonal winds that transport more cold water northward and finally suppress the upwelling of the subsurface warmer water.

Observing and simulating clouds and their radiative effects are challenging. Global climate models usually underestimate the supercooled liquid fraction of clouds, causing an underestimate of the albedo, especially over the Southern Ocean (Bodas-Salcedo et al., 2016, 2012; Cesana & Chepfer, 2013; Kay et al., 2016). CMIP5 models exhibit an erroneous net shortwave warming effect, which in part due to the inability to simulate the increase of low clouds associated with the poleward shift of the jet stream and storm-track (Boucher et al., 2013; Ceppi & Hartmann, 2015; Grise & Kelleher, 2021, 2014; Zelinka et al., 2018). As a result, less solar radiation is reflected, leading to an excess of surface downward shortwave radiation with a large positive bias of cloud radiation forcing. Excessive solar radiation entering the Southern Ocean leads to a positive SST bias. This can partly explain the failure of CMIP5 models in simulating the observed SST cooling in the Southern Ocean (Bodas-Salcedo et al., 2014; Hartery et al., 2020; Trenberth & Fasullo, 2010).

The insufficient cloud-radiative feedback in climate models can also be attributed to the uncertainty of aerosol-cloud interactions. That means aerosols will affect the formation of cloud through changing cloud droplet concentration and thus altering cloud albedo. One of the dominant aerosol sources over the Southern Ocean is sea spray (Murphy et al., 1998), which generated from wave breaking due to the strong wind at the ocean surface (Hartery et al., 2020). Korhonen et al. (2010) suggested substantial negative radiative feedback induced by emission of sea spray through increasing cloud drop concentrations in low-level clouds. The aerosols can also affect the cloud albedo via change in cloud phase. Using satellite-based observation, Sato and Inoue (2021) found that marine aerosols emitted from the Southern Ocean enhance low-level ice-cloud formation, especially in summer. Such change in cloud phase increases cloud albedo, which reduce the reflection of shortwave radiation. It might be linked to the incorrect cloud-radiative feedback over the Southern Ocean in climate models.

As for the cooling effect induced by the change of wind-driven Ekman advection, Ferreira et al. (2015) suggested, the warming below will eventually dominate over the cooling at sea surface from anomalous Ekman advection, with the sustained strengthened westerly winds induced by ozone depletion. However, the sharp decrease of ozone concentration has ceased around 2,000, and the ozone hole has started to heal since then (Eyring et al., 2007; Son et al., 2008). In addition, model predictions indicate that the increase of ozone concentration will continue in the next several decades. As a result, the climate effects and trends will likely be reversed due to the ozone recovery (Solomon et al., 2016; Zambri et al., 2021).

We also notice that the entrainment process contributes to a slight cooling trend in the central-east Pacific sector, but it is too small. In this study, the entrainment is calculated based on the change of the mixed layer depth, excluding the effect of net heat flux at the sea surface (another factor to cool the SST) in the calculation, which is included in the estimate of entrainment term in some studies (Dong et al., 2007; Ferreira et al., 2015; Vivier et al., 2010). The two major factors (the net shortwave radiation and wind-driven Ekman advection) identified here, together with other processes proposed in previous studies (i.e., the weakening of ocean deep convection and sea surface freshening due to an anthropogenic amplified hydrological cycle and ice sheet melting (Bintanja et al., 2013; Pauling et al., 2017; Zhang et al., 2019), may explain the observed SST cooling.

Data Availability Statement

All the data analyzed here are openly available. NOAA OISSTV2 data is provided by the NOAA/OAR/ESRL PSL, Boulder, Colorado, USA at <https://psl.noaa.gov/data/gridded/data.noaa.oisst.v2.html>, and NOAA ERSSTV5 data can be obtained at <https://psl.noaa.gov/data/gridded/data.noaa.ersst.v5.html>. HadISST1 data is available at <https://www.metoffice.gov.uk/hadobs/hadisst/>. ECMWF ORAS5 is available at <https://cds.climate.copernicus.eu/cdsapp#!/dataset/reanalysis-oras5?tab=form>. ERA5 monthly averaged data is provided by Copernicus Climate Change Service (C3S) Climate Data Store (CDS) (Accessed on 20-01-2021) 10.24381/cds.f17050d7 at <https://doi.org/10.24381/cds.f17050d7>. The monthly 10-ensemble mean of ECMWF data is provided by Copernicus

Climate Change Service (C3S) Climate Data Store (CDS) (Accessed on 08-02-2022) [10.24381/cds.f17050d7](https://doi.org/10.24381/cds.f17050d7) at <https://doi.org/10.24381/cds.f17050d7>. ISCCP H-series cloud data is provided by NOAA/NCEI at <https://www.ncei.noaa.gov/products/international-satellite-cloud-climatology>.

Acknowledgments

This research is supported by the National Key R&D Program of China (2018YFA0605901) and the National Natural Science Foundation of China (41830536 and 41941009).

References

- Alkama, R., Taylor, P. C., Garcia-San Martin, L., Douville, H., Duveiller, G., Forzieri, G., et al. (2020). Clouds damp the radiative impacts of polar sea ice loss. *The Cryosphere*, 14(8), 2673–2686. <https://doi.org/10.5194/tc-14-2673-2020>
- Armour, K. C., Marshall, J., Scott, J. R., Donohoe, A., & Newsom, E. R. (2016). Southern Ocean warming delayed by circumpolar upwelling and equatorward transport. *Nature Geoscience*, 9(7), 549–554. <https://doi.org/10.1038/ngeo2731>
- Bintanja, R., van Oldenborgh, G. J., Drijfhout, S. S., Wouters, B., & Katsman, C. A. (2013). Important role for ocean warming and increased ice-shelf melt in Antarctic sea-ice expansion. *Nature Geoscience*, 6(5), 376–379. <https://doi.org/10.1038/ngeo1767>
- Bitz, C. M., & Polvani, L. M. (2012). Antarctic climate response to stratospheric ozone depletion in a fine resolution ocean climate model. *Geophysical Research Letters*, 39(20). <https://doi.org/10.1029/2012GL053393>
- Bodas-Salcedo, A., Hill, P. G., Furtado, K., Williams, K. D., Field, P. R., Manners, J. C., et al. (2016). Large contribution of supercooled liquid clouds to the solar radiation budget of the Southern Ocean. *Journal of Climate*, 29(11), 4213–4228. <https://doi.org/10.1175/JCLI-D-15-0564.1>
- Bodas-Salcedo, A., Williams, K. D., Field, P. R., & Lock, A. P. (2012). The surface downwelling solar radiation surplus over the Southern Ocean in the Met Office model: The role of midlatitude cyclone clouds. *Journal of Climate*, 25(21), 7467–7486. <https://doi.org/10.1175/JCLI-D-11-00702.1>
- Bodas-Salcedo, A., Williams, K. D., Ringer, M. A., Beau, I., Cole, J. N. S., Dufresne, J.-L., et al. (2014). Origins of the solar radiation biases over the Southern Ocean in CFMIP2 models. *Journal of Climate*, 27(1), 41–56. <https://doi.org/10.1175/jcli-d-13-00169.1>
- Boucher, O., Randall, D., Artaxo, P., Bretherton, C., Feingold, G., Forster, P., et al. (2013). Clouds and aerosols. In T. F. Stocker (Ed.), *Climate change 2013: The physical science basis* (pp. 571–657). Cambridge University Press.
- Ceppi, P., & Hartmann, D. L. (2015). Connections between clouds, radiation, and midlatitude dynamics: A review. *Current Climate Change Reports*, 1(2), 94–102. <https://doi.org/10.1007/s40641-015-0010-x>
- Cesana, G., & Chepfer, H. (2013). Evaluation of the cloud thermodynamic phase in a climate model using CALIPSO-GOCCP. *Journal of Geophysical Research: Atmospheres*, 118(14), 7922–7937. <https://doi.org/10.1002/jgrd.50376>
- Charlock, T. P., & Ramanathan, V. (1985). The Albedo field and cloud radiative forcing produced by a general circulation model with internally generated cloud optics. *Journal of the Atmospheric Sciences*, 42(13), 1408–1429. [https://doi.org/10.1175/1520-0469\(1985\)042<1408:TAFACR>2.0.CO;2](https://doi.org/10.1175/1520-0469(1985)042<1408:TAFACR>2.0.CO;2)
- Dong, S., Gille, S. T., & Sprintall, J. (2007). An assessment of the Southern Ocean mixed layer heat budget. *Journal of Climate*, 20(17), 4425–4442. <https://doi.org/10.1175/JCLI4259.1>
- Eyring, V., Waugh, D. W., Bodeker, G. E., Cordero, E. C., Akiyoshi, H., Austin, J., et al. (2007). Multimodel projections of stratospheric ozone in the 21st century. *Journal of Geophysical Research: Atmospheres*, 112(D16), 1–24. <https://doi.org/10.1029/2006JD008332>
- Ferreira, D., Marshall, J., Bitz, C. M., Solomon, S., & Plumb, A. (2015). Antarctic Ocean and sea ice response to ozone depletion: A two-time-scale problem. *Journal of Climate*, 28(3), 1206–1226. <https://doi.org/10.1175/JCLI-D-14-00313.1>
- Fogt, R. L., & Marshall, G. J. (2020). The Southern Annular Mode: Variability, trends, and climate impacts across the Southern Hemisphere. *WIREs Climate Change*, 11(4), e652. <https://doi.org/10.1002/wcc.652>
- Grise, K. M., & Kelleher, M. K. (2021). Midlatitude cloud radiative effect sensitivity to cloud controlling factors in observations and models: Relationship with Southern Hemisphere jet shifts and climate sensitivity. *Journal of Climate*, 34(14), 5869–5886. <https://doi.org/10.1175/JCLI-D-20-0986.1>
- Grise, K. M., & Polvani, L. M. (2014). Southern Hemisphere cloud-dynamics biases in CMIP5 models and their implications for climate projections. *Journal of Climate*, 27(15), 6074–6092. <https://doi.org/10.1175/JCLI-D-14-00113.1>
- Hall, A., & Visbeck, M. (2002). Synchronous variability in the Southern Hemisphere atmosphere, sea ice, and ocean resulting from the Annular Mode. *Journal of Climate*, 15(21), 3043–3057. [https://doi.org/10.1175/1520-0442\(2002\)015<3043:SVTSH>2.0.CO;2](https://doi.org/10.1175/1520-0442(2002)015<3043:SVTSH>2.0.CO;2)
- Hartery, S., Toohey, D., Revell, L., Sellegri, K., Kuma, P., Harvey, M., & McDonald, A. J. (2020). Constraining the surface flux of sea spray particles from the Southern Ocean. *Journal of Geophysical Research: Atmospheres*, 125(4), e2019JD032026. <https://doi.org/10.1029/2019JD032026>
- Haumann, F. A., Gruber, N., & Münnich, M. (2020). Sea-ice induced Southern Ocean subsurface warming and surface cooling in a warming climate. *AGU Advances*, 1(2), e2019AV000132. <https://doi.org/10.1029/2019AV000132>
- Haumann, F. A., Gruber, N., Münnich, M., Frenger, I., & Kern, S. (2016). Sea-ice transport driving Southern Ocean salinity and its recent trends. *Nature*, 537(7618), 89–92. <https://doi.org/10.1038/nature19101>
- Hersbach, H., Bell, B., Berrisford, P., Biavati, G., Horányi, A., Muñoz Sabater, J., et al. (2019). ERA5 monthly averaged data on single levels from 1979 to present. Copernicus Climate Change Service (C3S) Climate Data Store (CDS). <https://doi.org/10.24381/cds.f17050d7>
- Huang, B., Thorne, P. W., Banzon, V. F., Boyer, T., Chepurin, G., Lawrimore, J. H., et al. (2017). Extended Reconstructed Sea Surface Temperature, version 5 (ERSSTv5): Upgrades, validations, and intercomparisons. *Journal of Climate*, 30(20), 8179–8205. <https://doi.org/10.1175/JCLI-D-16-0836.1>
- Jones, J. M., Fogt, R. L., Widmann, M., Marshall, G. J., Jones, P. D., & Visbeck, M. (2009). Historical SAM variability. Part I: Century-length seasonal reconstructions. *Journal of Climate*, 22(20), 5319–5345. <https://doi.org/10.1175/2009JCLI2785.1>
- Jones, J. M., Gille, S. T., Goosse, H., Abram, N. J., Canziani, P. O., Charman, D. J., et al. (2016). Assessing recent trends in high-latitude Southern Hemisphere surface climate. *Nature Climate Change*, 6(10), 917–926. <https://doi.org/10.1038/nclimate3103>
- Kay, J. E., Bourdages, L., Miller, N. B., Morrison, A., Yettella, V., Chepfer, H., & Eaton, B. (2016). Evaluating and improving cloud phase in the Community Atmosphere Model version 5 using spaceborne lidar observations. *Journal of Geophysical Research: Atmospheres*, 121(8), 4162–4176. <https://doi.org/10.1002/2015JD024699>
- Korhonen, H., Carslaw, K. S., Forster, P. M., Mikkonen, S., Gordon, N. D., & Kokkola, H. (2010). Aerosol climate feedback due to decadal increases in Southern Hemisphere wind speeds. *Geophysical Research Letters*, 37(2). <https://doi.org/10.1029/2009GL041320>
- Kostov, Y., Marshall, J., Hausmann, U., Armour, K. C., Ferreira, D., & Holland, M. M. (2017). Fast and slow responses of Southern Ocean Sea surface temperature to SAM in coupled climate models. *Climate Dynamics*, 48(5), 1595–1609. <https://doi.org/10.1007/s00382-016-3162-z>
- Levitus, S., Antonov, J. I., Boyer, T. P., Baranova, O. K., Garcia, H. E., Locarnini, R. A., et al. (2012). World Ocean heat content and thermocline sea level change (0–2,000 m), 1955–2010. *Geophysical Research Letters*, 39(10). <https://doi.org/10.1029/2012GL051106>

- Murphy, D. M., Anderson, J. R., Quinn, P. K., McInnes, L. M., Brechtel, F. J., Kreidenweis, S. M., et al. (1998). Influence of sea-salt on aerosol radiative properties in the Southern Ocean marine boundary layer. *Nature*, 392(6671), 62–65. <https://doi.org/10.1038/32138>
- Pauling, A. G., Bitz, C. M., Smith, I. J., & Langhorne, P. J. (2016). The response of the Southern Ocean and Antarctic sea ice to freshwater from ice shelves in an Earth system model. *Journal of Climate*, 29(5), 1655–1672. <https://doi.org/10.1175/JCLI-D-15-0501.1>
- Pauling, A. G., Smith, I. J., Langhorne, P. J., & Bitz, C. M. (2017). Time-dependent freshwater input from ice shelves: Impacts on Antarctic sea ice and the Southern Ocean in an Earth system model. *Geophysical Research Letters*, 44(20), 10454–10461. <https://doi.org/10.1002/2017GL075017>
- Purich, A., England, M. H., Cai, W., Sullivan, A., & Durack, P. J. (2018). Impacts of broad-scale surface freshening of the Southern Ocean in a coupled climate model. *Journal of Climate*, 31(7), 2613–2632. <https://doi.org/10.1175/JCLI-D-17-0092.1>
- Qiu, B., & Kelly, K. A. (1993). Upper-ocean heat balance in the Kuroshio extension region. *Journal of Physical Oceanography*, 23(9), 2027–2041. [https://doi.org/10.1175/1520-0485\(1993\)023<2027:UOHBTT>2.0.CO;2](https://doi.org/10.1175/1520-0485(1993)023<2027:UOHBTT>2.0.CO;2)
- Rayner, N. A., Parker, D. E., Horton, E. B., Folland, C. K., Alexander, L. V., Rowell, D. P., et al. (2003). Global analyses of sea surface temperature, sea ice, and night marine air temperature since the late nineteenth century. *Journal of Geophysical Research: Atmospheres*, 108(D14). <https://doi.org/10.1029/2002JD002670>
- Reynolds, R. W., Rayner, N. A., Smith, T. M., Stokes, D. C., & Wang, W. (2002). An improved in situ and satellite SST analysis for climate. *Journal of Climate*, 15(13), 1609–1625. [https://doi.org/10.1175/1520-0442\(2002\)015<1609:AIISAS>2.0.CO;2](https://doi.org/10.1175/1520-0442(2002)015<1609:AIISAS>2.0.CO;2)
- Rye, C. D., Marshall, J., Kelley, M., Russell, G., Nazarenko, L. S., Kostov, Y., et al. (2020). Antarctic glacial melt as a driver of recent Southern Ocean climate trends. *Geophysical Research Letters*, 47(11), e2019GL086892. <https://doi.org/10.1029/2019GL086892>
- Sallée, J. B., Speer, K. G., & Rintoul, S. R. (2010). Zonally asymmetric response of the Southern Ocean mixed-layer depth to the Southern Annular Mode. *Nature Geoscience*, 3(4), 273–279. <https://doi.org/10.1038/ngeo812>
- Sato, K., & Inoue, J. (2021). Seasonal change in satellite-retrieved lower-tropospheric ice-cloud fraction over the Southern Ocean. *Geophysical Research Letters*, 48, e2021GL095295. <https://doi.org/10.1029/2021GL095295>
- Sen Gupta, A., & England, M. H. (2006). Coupled ocean-atmosphere-ice response to variations in the Southern Annular Mode. *Journal of Climate*, 19(18), 4457–4486. <https://doi.org/10.1175/JCLI3843.1>
- Sen Gupta, A., Santos, A., Taschetto, A. S., Ummenhofer, C. C., Trevena, J., & England, M. H. (2009). Projected changes to the southern hemisphere ocean and sea ice in the IPCC AR4 climate models. *Journal of Climate*, 22(11), 3047–3078. <https://doi.org/10.1175/2008JCLI2827.1>
- Solomon, S., Ivy Diane, J., Kinnison, D., Mills Michael, J., Neely Ryan, R., & Schmidt, A. (2016). Emergence of healing in the Antarctic ozone layer. *Science*, 353(6296), 269–274. <https://doi.org/10.1126/science.aae0061>
- Son, S. W., Polvani, L. M., Waugh, D. W., Akiyoshi, H., Garcia, R., Kinnison, D., et al. (2008). The impact of stratospheric ozone recovery on the Southern Hemisphere westerly jet. *Science*, 320(5882), 1486–1489. <https://doi.org/10.1126/science.1155939>
- Thompson, D. W. J., Solomon, S., Kushner, P. J., England, M. H., Grise, K. M., & Karoly, D. J. (2011). Signatures of the Antarctic ozone hole in Southern Hemisphere surface climate change. *Nature Geoscience*, 4(11), 741–749. <https://doi.org/10.1038/ngeo1296>
- Trenberth, K. E., & Fasullo, J. T. (2010). Simulation of present-day and twenty-first-century energy budgets of the Southern Oceans. *Journal of Climate*, 23(2), 440–454. <https://doi.org/10.1175/2009JCLI3152.1>
- Vivier, F., Iudicone, D., Busdraghi, F., & Park, Y.-H. (2010). Dynamics of sea-surface temperature anomalies in the Southern Ocean diagnosed from a 2-D mixed-layer model. *Climate Dynamics*, 34(2), 153–184. <https://doi.org/10.1007/s00382-009-0724-3>
- Young, A. H., Knapp, K. R., Inamdar, A., Hankins, W., & Rossow, W. B. (2017). The International Satellite Cloud Climatology Project H-Series climate data record product. *Earth System Science Data*, 10, 1–21.
- Zambri, B., Solomon, S., Thompson, D. W. J., & Fu, Q. (2021). Emergence of Southern Hemisphere stratospheric circulation changes in response to ozone recovery. *Nature Geoscience*, 14(9), 638–644. <https://doi.org/10.1038/s41561-021-00803-3>
- Zelinka, M. D., Grise, K. M., Klein, S. A., Zhou, C., De Angelis, A. M., & Christensen, M. W. (2018). Drivers of the low-cloud response to poleward jet shifts in the North Pacific in observations and models. *Journal of Climate*, 31(19), 7925–7947. <https://doi.org/10.1175/JCLI-D-18-0114.1>
- Zhang, L., Delworth, T. L., Cooke, W., & Yang, X. (2019). Natural variability of Southern Ocean convection as a driver of observed climate trends. *Nature Climate Change*, 9(1), 59–65. <https://doi.org/10.1038/s41558-018-0350-3>
- Zuo, H., Balmaseda, M. A., Tietsche, S., Mogensen, K., & Mayer, M. (2019). The ECMWF operational ensemble reanalysis-analysis system for ocean and sea ice: A description of the system and assessment. *Ocean Science*, 15(3), 779–808. <https://doi.org/10.5194/os-15-779-2019>